NJC

New Journal of Chemistry

An international journal of the chemical sciences

www.rsc.org/njc

Volume 32 | Number 11 | November 2008 | Pages 1809–2052

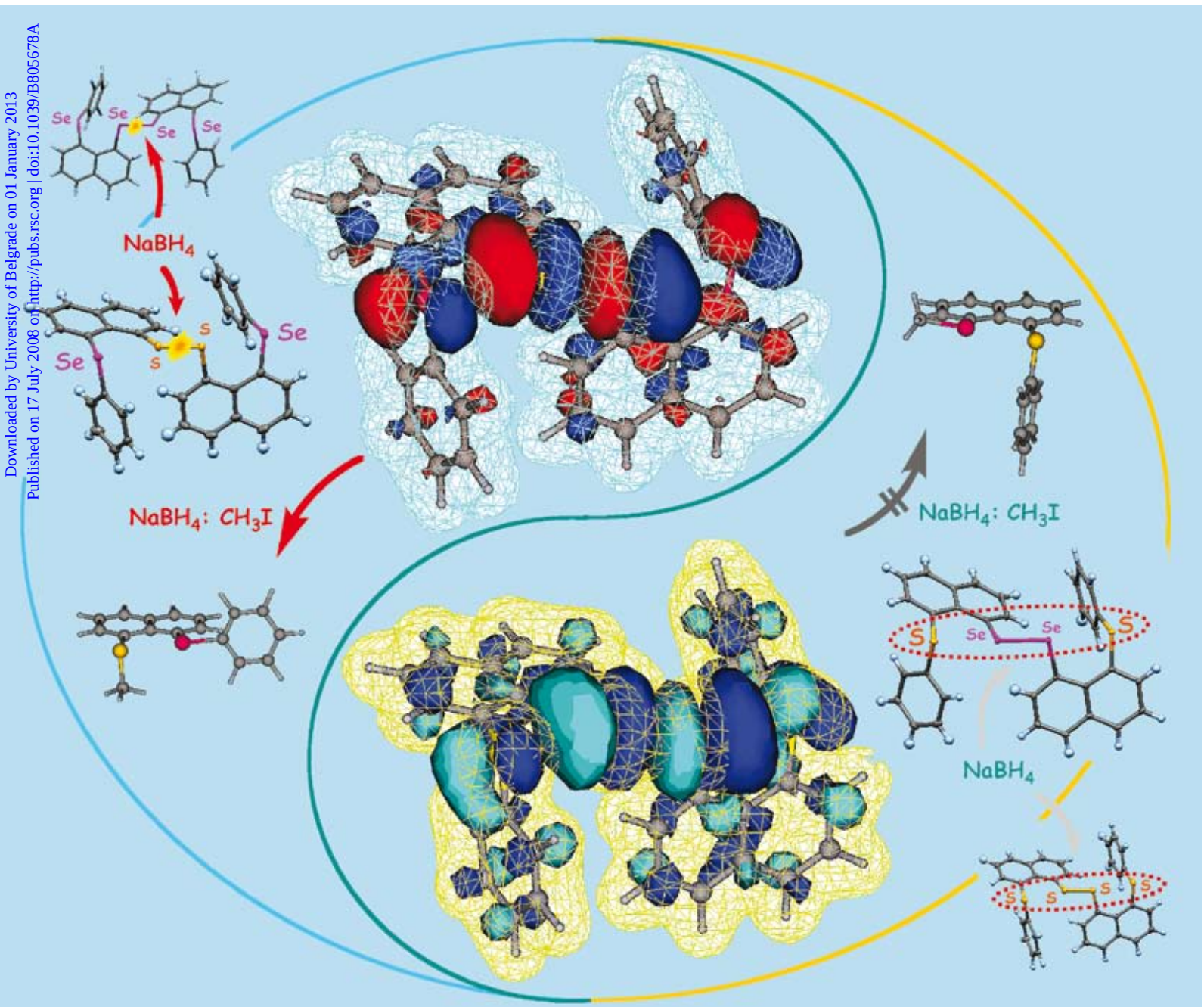

ISSN 1144-0546

RSC Publishing

CNRS CENTRE NATIONAL DE LA RECHERCHE SCIENTIFIQUE

PAPER

Nakanishi *et al.*

Extended hypervalent E′···E–E···E′ 4c–6e (E, E′ = Se, S) interactions: structure, stability and reactivity of 1-(8-PhE′$C_{10}H_6$)EE($C_{10}H_6$E′Ph-8′)-1′

Extended hypervalent E′···E–E···E′ 4c–6e (E, E′ = Se, S) interactions: structure, stability and reactivity of 1-(8-PhE′$C_{10}H_6$)EE($C_{10}H_6$E′Ph-8′)-1′†

Waro Nakanishi,*[a] Satoko Hayashi,[a] Sayuri Morinaka,[a] Takahiro Sasamori[b] and Norihiro Tokitoh[b]

Received (in Montpellier, France) 3rd April 2008, Accepted 23rd May 2008
First published as an Advance Article on the web 17th July 2008
DOI: 10.1039/b805678a

The structure, stability and reactivity of E′···E–E···E′ ($E_2E'_2$) 4c–6e are examined employing naphthalene 1,8-positions in 1-(8-PhE′$C_{10}H_6$)EE($C_{10}H_6$E′Ph-8′)-1′ [**1** (E = Se, E′ = S), **2** (E = S, E′ = Se), **3** (E = E′ = Se) and **4** (E = E′ = S)], together with 1-$C_{10}H_7$EE$C_{10}H_7$-1′ [**5** (E = Se) and **6** (E = S)]. Linear alignments of four Se_2S_2 atoms in **1** and **2** are confirmed by the X-ray analysis. **1** was not reduced by sodium borohydride, whereas **2** was, contrary to the expectation. Similarly, E–E in **3**, **5** and **6** were cleaved, whereas that in **4** was not, when allowed to react with $NaBH_4$ in aqueous THF. The reactivity of the E–E bonds in $E_2E'_2$ in **1–4** is not controlled by the central E atoms but by the outside E′ atoms. Quantum chemical (QC) calculations are performed on 1-(8-MeE′$C_{10}H_6$)EE($C_{10}H_6$E′Me-8′)-1′ (**13–16**: models of **1–4**, respectively), **5** and **6**, together with the related species. Conformers having $E_2E'_2$ 4c–6e (abbreviated by **BA**) are the global minima for **13**, **15** and **16**, which reproduces the observed structures: **BA** must be stabilized by the formation of $E_2E'_2$ 4c–6e. **14** (**AB**) with double n(S)···σ*(Se–C) 3c–4e interactions is the global minimum, which shows that σ*(Se–C) plays a crucial role to stabilize the 3c–4e in **AB**. The novel reactivity of E–E is considered based on the QC calculations.

Introduction

Extended hypervalent bonds [*m* center–*n* electron bonds (*m*c–*n*e: $m \geq 4$)][1–6] higher than 3c–4e are of current interest. They play an important role in physical, chemical and biological properties in the compounds containing the bonds.[1–5] Our strategy to construct the extended hypervalent bonds are to employ the interactions caused by direct orbital overlaps between nonbonded atoms.[3,4,6] The bonds are also shown to play an important role in the pharmacological activity[7] and development of electronic materials.[8,9] It is inevitable to control weak interactions to design materials of high functionalities, since they control fine structures and create delicate properties of materials.[10] The first member of the extended hypervalent bonds is 4c–6e. Compounds containing 4c–6e with linear four atoms have been gradually increased by the preparation and characterization of the compounds,[5] although they are sometimes not recognized as 4c–6e. The nature of 4c–6e[3] is demonstrated to be very different from that of 3c–4e.[10a,c,11,12] However, details in the reactivity of extended hypervalent bonds are still unclear, even recently.

The driving force for the linear alignment in 4c–6e is CT from two p-type lone pair orbitals of outside E′ atoms (n_p(E′)) to the central σ*(E–E) orbital. The interaction is analyzed by the 4c–6e model. Scheme 1 depicts the approximate molecular orbital model for E_4 4c–6e of the n_p(E)···σ*(E–E)···n_p(E) type. The CT in 4c–6e may correspond to ψ_2 of E_4 4c–6e.

Naphthalene 1,8-positions supply an excellent system to study the interactions between nonbonded atoms, since the nonbonded distances are close to the sum of van der Waals radii minus 1 Å for those of main group elements. Indeed, four atoms of the same kind construct extended hypervalent E_4 4c–6e, but those of the different kinds also form $E_2E'_2$ 4c–6e. Lots of possibilities would be derived from $E_2E'_2$ 4c–6e, where E′ = N,[5b,13] O,[14] S,[3d,15] Se,[3a,b] and halogens,[5f,16] even if E is limited to S and Se.

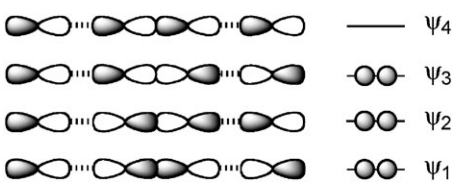

Scheme 1 Approximate MO model for E_4 4c–6e.

[a] *Department of Material Science and Chemistry, Faculty of Systems Engineering, Wakayama University, 930 Sakaedani, Wakayama, 640-8510, Japan. E-mail: nakanisi@sys.wakayama-u.ac.jp; Fax: +81 73 457 8253; Tel: +81 73 457 8253*
[b] *Institute for Chemical Research, Kyoto University, Gokasho, Uji, Kyoto, 611-0011, Japan*

† Electronic supplementary information (ESI) available: Cartesian coordinates for optimized structures of **5**, **6** and **13–20**. CCDC reference numbers 626066 for **1** and 626067 for **2**. For ESI and crystallographic data in CIF or other electronic format see DOI: 10.1039/b805678a

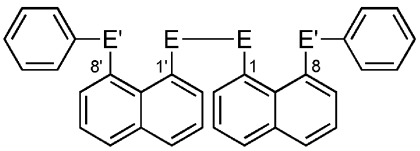

1 (E = Se, E' = S), **2** (E = S, E' = Se)
3 (E = E' = Se), **4** (E = E' = S)

Chart 1 Naphthalene system containing $E_2E'_2$ 4c–6e (E, E′ = Se, S).

We investigated the structure, stability and reactivity of $E_2E'_2$ 4c–6e in bis[8-(phenylthio)naphthyl] 1,1′-diselenide (**1**) and bis[8-(phenylselanyl)naphthyl] 1,1′-disulfide (**2**), together with bis[8-(phenylselanyl)naphthyl] 1,1′-diselenide (**3**)[3a–c] and bis[8-(phenylthio)naphthyl] 1,1′-disulfide (**4**)[3d] (Chart 1).[17] Those of 1,1′-dinaphthyl diselenide (**5**)[18,19] and 1,1′-dinaphthyl disulfide (**6**)[19] are also discussed for convenience of comparison.

During the course in the preparation of **1** and **2**, we found the novel reactivity of **1**, relative to **2**, toward the reduction with sodium borohydride: **1** was not reduced by sodium borohydride, whereas **2** was reduced, although **2** is expected to be less reactive. The observation is the first typical example caused by $E_2E'_2$ 4c–6e (E, E′ = Se, S), to the best of our knowledge. The reactivity must arise from the unique bonding scheme of Se_2S_2 4c–6e in **1** and **2**. Compilation of the results, it is summarized that the reactivity of the E–E bonds in E′···E–E···E′ 4c–6e toward the reduction with sodium borohydride is not controlled by the central E atoms but by the outside E′ atoms in 1-(8-PhE′$C_{10}H_6$)EE($C_{10}H_6$E′Ph-8′)-1′.

Here, we report the properties of **1** and **2**, together with those of **3–6**. The structures are determined for **1** and **2**. The stability is also clarified, which must be closely related to the novel reactivity of **1–4**. Quantum chemical (QC) calculations are employed to understand the unique properties of 1-(8-PhE′$C_{10}H_6$)EE($C_{10}H_6$E′Ph-8′)-1′.

Results and discussion

Survey of the E–E bond reduction

An almost equimolar mixture of **1** and **2** was obtained in the reaction of the naphtho[1,8-*c*,*d*]-1,2-selenathiolate dianion with excess benzenediazonium chloride in aqueous THF at 5 °C. 1-(Methylthio)-8-(phenylselanyl)naphthalene (**7**) was isolated, together with **1**, after treatment of the mixture with excess sodium borohydride, followed by excess methyl iodide. 1-(Methylselanyl)-8-(phenylthio)naphthalene (**8**) and **2** were not detected in the reaction mixture, contrary to the expectation. 1-(Methylselanyl)-8-(phenylselanyl)-naphthalene (**9**)[3b,c] was isolated in the reduction of **3** under the conditions, whereas 1-(methylthio)-8-(phenylthio)-naphthalene (**10**) was not obtained in the reduction of **4**; eqns (1) and (2) show the reactions.[3] As shown in eqn (3), **5** and **6** gave 1-(methylselanyl)naphthalene (**11**) and 1-(methylthio)naphthalene (**12**), respectively, under similar conditions of the reduction. Table 1 summarizes the reactivity of **1–6** toward sodium borohydride.

Table 1 Reduction of **1–6** with $NaBH_4$, followed by excess MeI[a]

Entry	Compound	Product	Reactivity	Yield[b] (%)
1	**1** (SSeSeS)	**1**[c]	—	98[c]
2	**2** (SeSSSe)	**7**	++	96
3	**3** (SeSeSeSe)	**9**	++	97
4	**4** (SSSS)	**4**[c]	—	95[c]
5	**5** (SeSe)	**11**	+++	>99
6	**6** (SS)	**12**	+++	>99

[a] Dichalcogenide (25 mmol) was solved in aqueous THF, then added sodium borohydride (200 mmol). After stirring for 20 min at 30 °C, excess methyl iodide (100 mmol) was added. [b] Isolated yield. [c] Recovered.

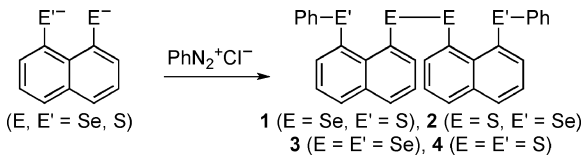

(E, E' = Se, S)

1 (E = Se, E' = S), **2** (E = S, E' = Se)
3 (E = E' = Se), **4** (E = E' = S)

(1)

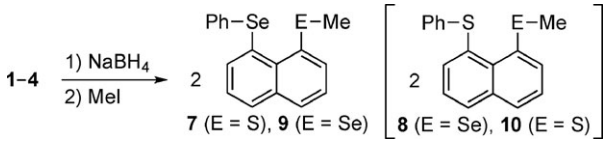

7 (E = S), **9** (E = Se) **8** (E = Se), **10** (E = S)

(2)

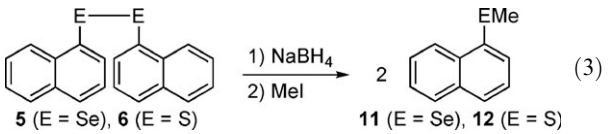

5 (E = Se), **6** (E = S) **11** (E = Se), **12** (E = S)

(3)

The disulfide **2** was independently prepared by the reduction of 1-(8-PhSe$C_{10}H_6$)SS_2S($C_{10}H_6$SePh-8′)-1′ with $NaBH_4$ in ethanol, since **2** was not obtained in the reaction shown by eqn (1). Eqn (4) exhibits the reaction. The tetrasulfide was obtained in the reaction of 1-Br-8-(PhSe)$C_{10}H_6$ with magnesium in diethyl ether, followed by addition of excess sulfur,[20] although the tetrasulfide was contaminated by **2** to some extent. **2** was confirmed to give **7** in the reduction with $NaBH_4$ in aqueous THF, followed by MeI.

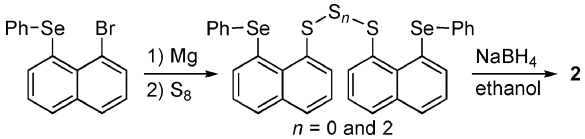

(4)

The reactivity of E–E in **1–6** is summarized as follows: (1) The E–E bonds (E = S and Se) in **5** and **6** are cleaved by sodium borohydride in aqueous THF. (2) The reactivity of the E–E bonds (E_2 σ(2c–2e)) dramatically changes if the bonds are incorporated in σ(4c–6e) of the $n_p(E')\cdots\sigma^*(E–E)\cdots n_p(E)$ type. (3) The reactivity of the E–E bonds is not controlled by the central E atoms but by the outside E′ atoms. The E–E bonds are cleaved by $NaBH_4$, when E′ = Se but not if E′ = S.

Why such a unique reactivity is observed in E–E of **1–6**? The reactivity of the compounds is elucidated, together with the structures and the stability.

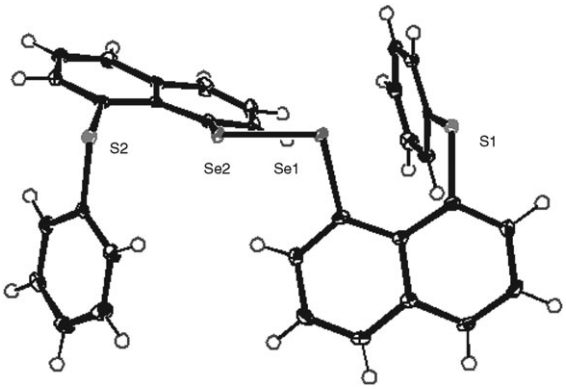

Fig. 1 Structure of **1** with displacement ellipsoids shown at the 50% probability level. Selected bond lengths (Å) and angles (°): Se1–Se2 2.3561(6), S1–Se1 3.0122(9), S2–Se2 2.9495(9); S1–Se1–Se2 169.622(13), Se1–Se2–S2 179.225(12).

Structures of 1 and 2

The X-ray crystallographic analyses are carried out for suitable single crystals of **1** and **2**, obtained *via* slow evaporation of hexane–dichloromethane solutions. Figs. 1 and 2 show the structures of **1** and **2**, respectively. The Se···S distances in **1** are 3.0122(9) and 2.9495(9) Å, which are shorter than the sum of the van der Waals radii of Se and S[21] by 0.69–0.75 Å. The structure of **2** is essentially the same as that of **1**, although the positions of S and Se are exchanged. The S···Se distances in **2** are 3.0458(7) and 3.0662(7) Å, which are shorter than the sum of the van der Waals radii by 0.63–0.65 Å. The distances are slightly shorter in **1**, relative to the case of **2** (by 0.075 Å in the average).

Structures of the naphthalene system are well classified using type **A** (**A**), **B** and **C**, where the Se–C_{Ar} bond is placed almost perpendicular to the naphthyl plane in **A**, the bond is located on the plane in **B** and **C** is the intermediate between **A** and **B**. Scheme 2 shows the notation.[3c,10a,c,12] Plausible conformers of **1–4** are **A**(1)**A**(1′)**A**(8)**A**(8′) (abbreviated by **AA**), **A**(1)**A**(1′)**B**(8)**B**(8′) (**AB**) and **B**(1)**B**(1′)**A**(8)**A**(8′) (**BA**). Scheme 3 illustrates the **AA**, **AB** and **BA** structures. The frameworks of the optimized

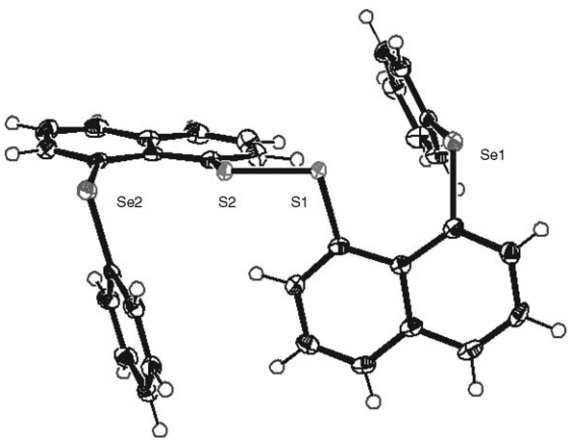

Fig. 2 Structure of **2** with displacement ellipsoids shown at the 50% probability level. Selected bond lengths (Å) and angles (°): S1–S2 2.0706(9), S1–Se1 3.0458(7), S2–Se2 3.0662(7); Se1–S1–S2 167.98(3), S1–S2–Se2 168.12(3).

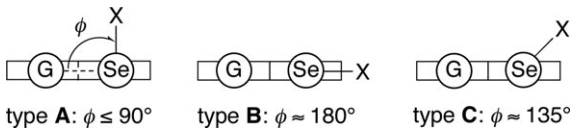

Scheme 2 Types **A**, **B** and **C** in naphthalene system.

structures for 1-(8-MeS$C_{10}H_6$)SeSe($C_{10}H_6$SMe-8′)-1′ (**13**: Chart 2) at the B3LYP level are employed for the illustration, although the H_{Me} atoms are removed. The observed structures are all **BA** for **1–4**. The results strongly suggest that **BA** with $E_2E'_2$ 4c–6e (E, E′ = S, Se) are more stable than **AB** constructed by double E···E′–C 3c–4e and **AA** with double E···E′ 2c–4e, although the crystal packing effect must also play an important role to determine the structures.

Why are **BA** observed in **1–4**? Why is the reactivity of E–E in **1–4** affected so much by E′? The reason is considered based on the QC calculations, next.

QC Calculations

QC calculations are performed on 1-(8-MeE′$C_{10}H_6$)EE-($C_{10}H_6$E′Me-8′)-1′ (E, E′ = Se, S) (**13–16**: models of **1–4**, respectively), together with **5**, **6** and 1-(8-MeE′$C_{10}H_6$)E^- (**17–20**). **17–20** are the anions formed from **13–16**, respectively, by the E–E bond reduction (Chart 2). Calculations are performed using the Gaussian 03 program[22] at the DFT (B3LYP)[23,24] and MP2[25] levels.

Table 2 collects selected bond lengths, angles and torsional angles of the optimized structures for **BA** of **13–16**, together with the observed values of **1–4**, necessary for the discussion. Table 3 shows the results for **13–16**, **5** and **6**: Energies on the energy potential surface and the sum of electronic and thermal free energies at 273.16 K are given for the values at the B3LYP level and those only on the energy potential surface at the MP2 level. The sum of electronic and thermal free energies corresponds to the Gibbs free energy ($G = H–TS$), which contains the zero-point correction. Natural bond orbital (NBO) analysis[26,27] are performed on **AB** and **BA** of **13–16** at the MP2 level. Table 4 collects the results. Table 5 shows the energies for **17–20** on the energy potential surface at the both levels.

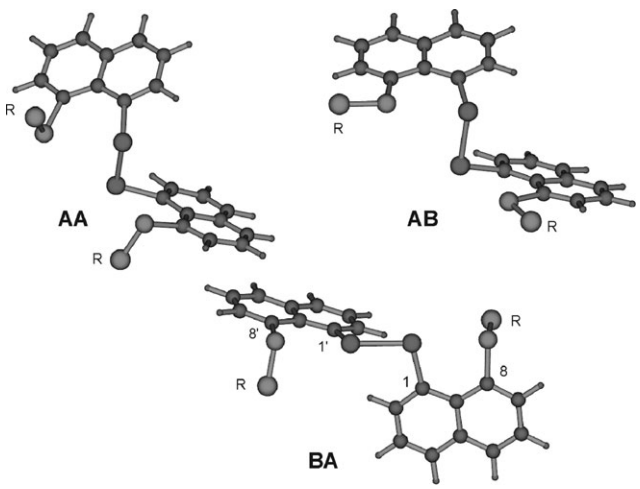

Scheme 3 **AA**, **AB** and **BA** structures in **1–4** and **13–16**. Frameworks for optimized structures of **13** being employed with R in replace of Me.

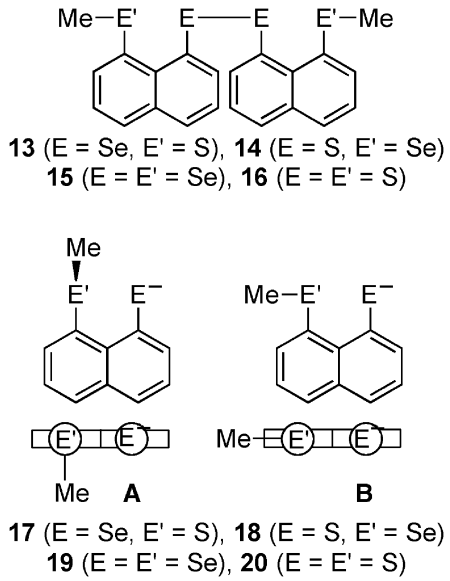

Chart 2 Calculated species.

Table 5 also contains the relative energies assuming that of **AB** as the standard for each.

Optimized structures around $E_2E'_2$ 4c–6e (E, E′ = Se, S)

Compounds **13–16** are the models of **1–4**, respectively. The selected bond lengths, angles and torsional angles of the optimized structures for **BA** of **13–16** are collected in Table 2, which correspond to the observed values for **BA** of **1–4**. The values optimized at the MP2 level are very close to those of observed values, while **13–16** have two E′–Me groups for each whereas **1–4** have two E′–Ph groups. Although the r(E–E) and ϕ(CEEC) values optimized at the B3LYP level are longer and smaller than those of observed values, structures optimized at the B3LYP level also reproduced the observed ones as a whole.

Table 3 Energies for **AA**, **AB** and **BA** of **13–16**, together with those for **A** and **B** of **5** and **6**[a]

Compound	ΔE(**AA**)[b,c]	E(**AB**)[d]	ΔE(**AB**)[b,e]	ΔE(**BA**)[b,f]
Calculated at the B3LYP level[g]				
13 (SSeSeS)	5.8	−6448.8883	0.0	−26.8
	8.1[h]	−6448.6170[h]	0.0[h]	−28.6[h]
14 (SeSSSe)	21.0	−6448.8768	0.0[i]	10.2[j]
	18.4[h]	−6448.6048[h]	0.0[hk]	3.4[hl]
15 (SeSeSeSe)	22.3	−10455.5558	0.0	−11.0
	19.7[h]	−10455.2880[h]	0.0[h]	−21.0[h]
16 (SSSS)	7.1	−2442.2098	0.0	−4.2
	7.1[h]	−2441.9337[h]	0.0[h]	−4.5[h]
5 (SeSe)[m]		−5573.8510	0.0	11.8
		−5573.6273[h]	0.0[h]	13.9[h]
6 (SS)[m]		−1567.1702	0.0	10.2
		−1566.9420[h]	0.0[h]	11.8[h]
Calculated at the MP2 level[n]				
13 (SSeSeS)		−6439.7877	0.0	−21.0
14 (SeSSSe)		−6439.7788	0.0[o]	17.9[p]
15 (SeSeSeSe)		−10444.5897	0.0	−0.3
16 (SSSS)		−2434.9772	0.0	−0.2
5 (SeSe)[m]		−5566.3505	0.0	25.3
6 (SS)[m]		−1561.5384	0.0	22.5

[a] Energies on the energy potential surface are given unless otherwise noted. [b] In kJ mol^{-1}. [c] ΔE(**AA**) = E(**AA**) − E(**AB**). [d] In au. [e] Taken as the standard for each. [f] ΔE(**BA**) = E(**BA**) − E(**AB**). [g] The 6-311+G(d) basis sets being employed for Se and S and the 6-311G(d) basis sets for C and H. [h] Sum of electronic and thermal free energies at 273.16 K. [i] 30.2 kJ mol^{-1} from **13** (**AB**). [j] 67.2 kJ mol^{-1} from **13** (**BA**). [k] 32.0 kJ mol^{-1} from **13** (**AB**). [l] 64.0 kJ mol^{-1} from **13** (**BA**). [m] Data for **5** (**A**) and **6** (**A**) are given in the column of **AB** and those for **5** (**B**) and **6** (**B**) are in that of **BA**. [n] The 6-311+G(d) basis sets being employed for Se and S and the 4-31G(d) method for C and H. [o] 23.4 kJ mol^{-1} from **13** (**AB**). [p] 62.1 kJ mol^{-1} from **13** (**BA**).

The optimized structures of **AA**, **AB** and **BA** of **13** at the B3LYP level are employed in Scheme 3, although the methyl protons

Table 2 Selected bond lengths, angles and torsional angles of the optimized structures for **BA** of **13–16**, together with those of **1–4**

Compound	(E, E′)	r(E–E)/Å	r(E···E′)/Å	∠(E′EE)/°	ϕ(CEEC)/°
Calculated at the B3LYP level[a]					
13 (**BA**)[b]	(Se, S)	2.4264	3.0125[c]	174.83	85.68
14 (**BA**)[b]	(S, Se)	2.1614	3.0587[c]	167.31	85.56
15 (**BA**)	(Se, Se)	2.4476	3.0849	172.68	85.94
16 (**BA**)	(S, S)	2.1461	2.9764	169.30	84.68
Calculated at the MP2 level[d]					
13 (**BA**)[e]	(Se, S)	2.3680	3.0134[f]	175.68	87.09
14 (**BA**)[e]	(S, Se)	2.0899	3.0792[f]	171.14	88.74
15 (**BA**)	(Se, Se)	2.3806	3.0887	174.54	89.31
16 (**BA**)	(S, S)	2.0814	3.0043	172.61	86.33
Determined by X-ray analysis[g]					
1 (**BA**)	(Se, S)	2.356	2.981[h]	174.43	−91.50
2 (**BA**)	(S, Se)	2.071	3.056[h]	168.06	−81.34
3 (**BA**)[i]	(Se, Se)	2.365	3.053	173.78	91.4
4 (**BA**)[j]	(S, S)	2.055	2.988	167.3	−89.0

[a] The 6-311+G(d) basis sets being employed for Se and S and the 6-311G(d) basis sets for C and H. [b] E(**14** (**BA**)) − E(**13** (**BA**)) = 67.2 kJ mol^{-1}. [c] r(E···E′: **14** (**BA**)) − r(E···E′: **13** (**BA**)) = 0.046 Å. [d] The 6-311+G(d) basis sets being employed for Se and S and the 4-31G(d) basis sets for C and H. [e] E(**14** (**BA**)) − E(**13** (**BA**)) = 62.1 kJ mol^{-1}. [f] r(E···E′: **14** (**BA**)) − r(E···E′: **13** (**BA**)) = 0.066 Å. [g] Averaged values are shown, if necessary. [h] r(E···E′: **2** (**BA**)) − r(E···E′: **1** (**BA**)) = 0.075. [i] Ref. 3*a*,*b*. [j] Ref. 3*c*.

Table 4 Results of NBO analysis for **AB** and **BA** of **13–16**, at the MP2 level[a,b]

Compound	NBO(*i*)[c]	NBO(*j*)[d]	$E(2)$/kcal mol^{-1}	$[E(j) - E(i)]$/au	$F(i,j)$/au
13 (BA)[e]	n_p(S)	σ*(Se–Se)	13.87	0.54	0.077
14 (BA)[f]	n_p(Se)	σ*(S–S)	9.22	0.56	0.064
15 (BA)[g]	n_p(Se)	σ*(Se–Se)	15.89	0.51	0.080
16 (BA)[h]	n_p(S)	σ*(S–S)	8.17	0.58	0.062
13 (AB)	n_p(Se)	σ*(S–C)	5.27	0.69	0.059
14 (AB)[i]	n_p(S)	σ*(Se–C)	9.32	0.67	0.071
15 (AB)[j]	n_p(Se)	σ*(Se–C)	9.19	0.64	0.069
16 (AB)	n_p(S)	σ*(S–C)	5.77	0.73	0.059

[a] Second-order perturbation of Fock matrix (threshold being 0.50 kcal mol^{-1}). [b] The 6-311+G(d) basis sets being employed for Se and S and the 4-31G(d) basis sets for C and H. [c] Donor orbitals. [d] Acceptor orbitals. [e] $E(2: n_s(S) \rightarrow \sigma^*(Se–Se))$ = 1.16 kcal mol^{-1}. [f] $E(2: n_s(Se) \rightarrow \sigma^*(S–S))$ = 0.60 kcal mol^{-1}. [g] $E(2: n_s(Se) \rightarrow \sigma^*(Se–Se))$ = 1.11 kcal mol^{-1}. [h] $E(2: n_s(S) \rightarrow \sigma^*(S–S))$ = 0.62 kcal mol^{-1}. [i] $E(2: n_s(S) \rightarrow \sigma^*(Se–C))$ = 0.83 kcal mol^{-1}. [j] $E(2: n_s(Se) \rightarrow \sigma^*(Se–C))$ = 0.67 kcal mol^{-1}.

Table 5 Energies of **A** and **B** in **17–20**[a]

	E(**A**)[b]	ΔE(**B**)[c,d]	E(**A**)[b]	ΔE(**B**)[c,d]
Anion	B3LYP[e]		MP2[f]	
17	−3224.4944	−9.5	−3219.9179	1.4
18	−3224.4911	−32.0	−3219.9095	−17.4
19	−5227.8258	−30.5	−5222.3162	−17.2
20	−1221.1589	−11.6	−1217.5105	0.7

[a] Energies on the energy potential surface are given. [b] In au. [c] ΔE(**B**) = E(**B**) − E(**A**). [d] In kJ mol^{-1}. [e] The 6-311+G(d) basis sets being employed for Se and S and the 6-311G(d) basis sets for C and H. [f] The 6-311+G(d) basis sets being employed for Se and S and the 4-31G(d) basis sets for C and H.

are removed to show R in place of Me. Optimized structures at the MP2 levels are also employed in Schemes 4 and 5.

The nonbonded r(Se···S) value for **14** (**BA**) is predicted to be shorter than that for **13** (**BA**) at the B3LYP and MP2 levels by 0.046 and 0.066 Å, respectively. The values must correspond to the observed difference of 0.075 Å between **2** (**BA**) and **1** (**BA**).[28] The smaller length must arise from the stronger the n_p(S)···σ*(Se–Se)···n_p(S) 4c–6e interaction relative to the n_p(Se)···σ*(S–S)···n_p(Se) 4c–6e interaction. The energy differences are evaluated to be 67 and 62 kJ mol^{-1} at the B3LYP and MP2 levels, respectively (see also Table 3 and Scheme 4).[28]

Stability of $E_2E'_2$ 4c–6e (E, E′ = Se, S)

As mentioned above, **BA**, **AB** and **AA** are optimized to be stable for **13–16** and **A** and **B** for **5** and **6**, when calculated at the B3LYP level (Tables 2 and 3). DFT calculations reveal that **BA** and **AB** are more stable than **AA** in **13–16**. **BA** are the global minimum for **13**, **15** and **16**, although the energy difference is small in **16**. **AB** is predicted to be the global minimum in **14**. Thermal effect operates to stabilize **BA** more than **AB** by up to 10 kJ mol^{-1}. **5** (**A**) is predicted to be more stable than the **5** (**B**) by *ca.* 10 kJ mol^{-1}, so is **6** (**A**) than **6** (**B**).[29] The MP2 calculations are performed on the key conformers (**AB** and **BA**) in **13–16**, together with **A** and **B** for **5** and **6**. Results at the MP2 level are essentially the same as those at the B3LYP level, although **BA** are less stabilized than **AB** at the MP2 level for **13–16**. **B** are less stabilized than **A** by 11–14 kJ mol^{-1} for **5** and **6** at the MP2 level.

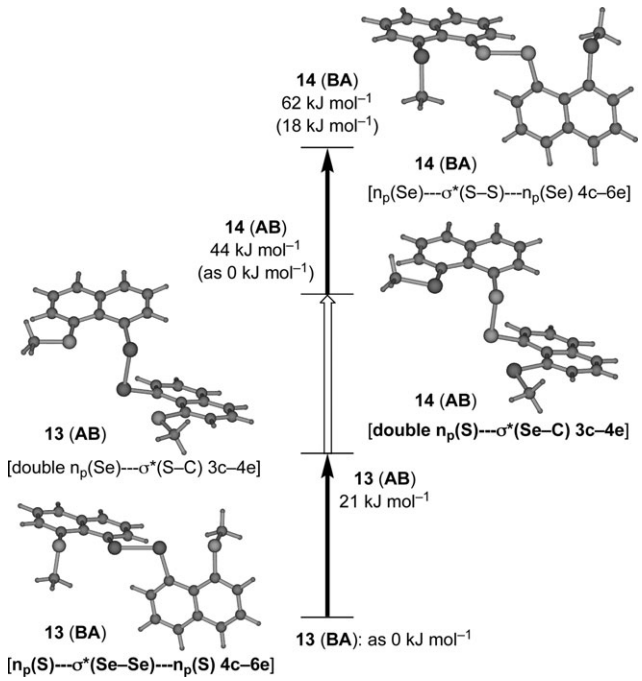

Scheme 4 Relative stability of $n_p(E')\cdots\sigma^*(E–E)\cdots n_p(E')$ 4c–6e *vs.* double $n_p(E)\cdots\sigma^*(E'–C)$ 3c–4e in **13** and **14**, predicted at the MP2 level.

The observed structure of **1** is **BA** in crystals, which correspond to **13** (**BA**) in the calculations. The calculated results well reproduce the observed structure of **1**, since **13** (**BA**) is predicted to be more stable than **13** (**AB**) by 21 kJ mol^{-1} at the MP2 level. (The optimized structure of **13** (**BA**) employed in Scheme 4 is very similar to the observed structure of **1**, although Ph in **1** are replaced by Me in **13**.) **14** is the model of **2**. The optimized structure of **14** (**BA**) also reproduces the observed structure of **2** (see, Fig. 2 and Scheme 4). However, **14** (**BA**) is predicted to be less stable than **14** (**AB**) by 18 kJ mol^{-1} at the MP2 level or 10 kJ mol^{-1} at the B3LYP level. The energy difference becomes to smaller if the thermal effect is considered as predicted at the B3LYP level (3 kJ mol^{-1}). Nevertheless, **14** (**BA**) is predicted to be still less stable than **14** (**AB**) containing the thermal effect at the B3LYP level.

The crystal packing effect is expected to play an important role to determine the structure of **2**. The effect must operate to stabilize **14** (**BA**) more than **14** (**AB**) by over the calculated energy

difference. Similar discrepancy is also observed in the structure of **6**. **5** (**A**) and **6** (**A**) are predicted to be more stable than **5** (**B**) and **6** (**B**), respectively, by 23–25 kJ mol^{-1} at the MP2 level or 10–14 kJ mol^{-1} at the B3LYP level. Indeed, **5** (**A**) is detected in crystals, but **6** is observed as **B**, irrespective of the predictions.[30]

15 and **16** are the models of **3** and **4**, respectively: **3** (**BA**) and **4** (**BA**) are observed in crystals. **15** (**BA**) is predicted to be slightly more stable than **15** (**AB**) at the MP2 level whereas the former is more stable than the latter by 21 kJ mol^{-1} if thermal effect is considered at the B3LYP level. The observed structure of **4** (**BA**) seems to be reproduced by the calculations: **16** (**BA**) is predicted to be slightly more stable than **16** (**AB**), although the predicted energy difference is less than 5 kJ mol^{-1} at the both level even if the thermal effect is considered. **4** (**BA**) must be more stable than **4** (**AB**) under the experimental conditions, since the **BA** structure is observed in **4′** which have the methoxy or nitro groups at the phenyl *p*,*p′*-positions in **4** (Chart 3). The extended form such as **B** in **6** and **BA** in **1–4** would be much stabilized by the crystal packing effect than expected. The phenyl groups may also operate to stabilize the **BA** form.

Scheme 4 illustrates the energy differences between **BA** and **AB** (ΔE(**BA**) = E(**BA**) − E(**AB**)), which corresponds to the formation of n_p(E′)···σ*(E–E)···n_p(E′) 4c–6e from double n_p(E)···σ*(E′–C) 3c–4e.[31] **13** (**BA**) with S···Se–Se···S 4c–6e is predicted to be more stable than **13** (**AB**) by 21 kJ mol^{-1} at the MP2 level. It is worthwhile to comment that **14** (**AB**) with double n_p(S)···σ*(Se–C) 3c–4e is predicted to be more stable than **14** (**BA**) with Se···S–S···Se 4c–6e by 18 kJ mol^{-1} if calculated at the same level. The observed nonbonded Se···S distances in **1** (**BA**) are slightly shorter than those in **2** (**BA**) (by 0.075 Å), which would be the reflection of the energy profiles in **13** and **14**. Whereas the stability of the n_p(E′)···σ*(E–E)···n_p(E′) 4c–6e in **BA** is mainly controlled by the central σ*(E–E), the stability of the n_p(E)···σ*(E′–C) 3c–4e in **AB** must be determined by σ*(E′–C) (Table 3). Namely, the stability of **BA** are controlled by σ*(E–E) but that of **AB** by σ*(E′–C) in **13–16**.

13 and **14** are isomers with each other. Therefore, the energies of the conformers in **13** and **14** can be directly compared. As shown in Scheme 4, **13** (**BA**) is the global minimum in **13** and **14**: **13** (**BA**) is more stable than **14** (**BA**) by 62 kJ mol^{-1} at the MP2 level (67 kJ mol^{-1} at the DFT level) (Table 2). The lesser stability of **14** (**BA**) *versus* higher stability of **13** (**BA**) explains the high reactivity of **2**, relative to **1**, toward the reduction under the conditions.

After elucidation of the structures and the stability of the $E_2E'_2$ 4c–6e (E, E′ = Se, S), the driving force for the formation of the 4c–6e is examined based on the NBO analysis.

Driving force for the formation of $E_2E'_2$ 4c–6e (E, E′ = Se, S)

The CT interactions can be evaluated as the second order perturbation of Fock matrix as defined by eqn (5). For each donor NBO (*i*) and acceptor NBO (*j*), the stabilization energy $E(2)$ associated with delocalization is estimated as eqn (5), where q_i is the donor orbital occupancy, ε_j and ε_i are diagonal elements (orbital energies) and $F(i,j)$ is the off-diagonal NBO Fock matrix element.

$$E(2) = \Delta E_{ij} = q_i F(i,j)^2/(\varepsilon_j - \varepsilon_i) \quad (5)$$

The energy lowering effect by the CT interactions of the n_p(E′)···σ*(E–E) type in **BA** and the n_p(E)···σ*(E′–C) type in **AB** are collected in Table 4. The n_p(E′)···σ*(E–E) interaction corresponds to half of the $E_2E'_2$ 4c–6e interaction in **BA** and there are two n_p(E)···σ*(E′–C) interactions in **AB**. The contributions from n_s are given in the footnotes of Table 4. The effect of the CT from n_p is discussed, since that from n_s is small and would not perturb the discussion.

The n_p(E′)···σ*(E–E) interactions in **13** (**BA**: E = Se, E′ = S) and **15** (**BA**: E = E′ = Se) stabilize the system by 13.9 and 15.9 kcal mol^{-1}, respectively, but the interactions in **14** (**BA**: E = S, E′ = Se) and **16** (**BA**: E = E′ = S) do only by 9.2 and 8.2 kcal mol^{-1}, respectively. The results show that the σ*(Se–Se) bonds in **13** (**BA**) and **15** (**BA**) operate to form and stabilize the 4c–6e bonds. On the other hand, the n_p(E)···σ*(E′–C) interactions in **14** (**AB**: E = S, E′ = Se) and **15** (**AB**: E = E′ = Se) stabilize the system by 9.3 and 9.2 kcal mol^{-1}, respectively, but the interactions in **13** (**AB**: E = Se, E′ = S) and **16** (**AB**: E = E′ = S) do only by 5.3 and 5.8 kcal mol^{-1}, respectively. The results show that the σ*(Se–C) bonds in **14** (**AB**) and **15** (**AB**) operate to stabilize the 3c–4e bonds.

The **AB** structure was not detected even in **14**. However, **AB** would be detected if a more suitable system is investigated, since the effect of the n_p(E′)···σ*(E–E) interaction is very close to that of the n_p(E)···σ*(E′–C) interaction in **14**.[32]

How is the unique reactivity of $E_2E'_2$ 4c–6e in **1–4** explained as a whole? The reactivity is considered based on QC calculations, next.

Reactivity of $E_2E'_2$ 4c–6e (E, E′ = Se, S)

The reactivity of **13–16** derived from **1–4** could be related to the stability of the intermediate anions [1-(8-MeE′$C_{10}H_6$)E$^-$] (**17–20**), produced by the reduction of **13–16**. As shown in Table 5, **18** (**B**) and **19** (**B**) are more stable than **18** (**A**) and **19** (**A**), respectively, by 17 kJ mol^{-1}, whereas the stability of **A**

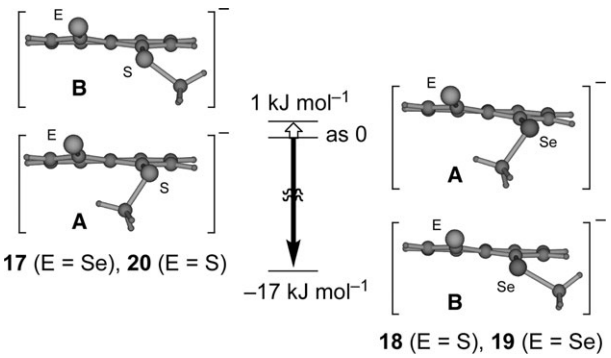

Scheme 5 Relative stability of anions (**17–20**) produced by the reduction of the E–E bonds in **13–16**: The **B** forms are much more stable than **A** for **18** and **19** whereas the stability is almost the same for **17** and **20**. Values are predicted at the MP2 level.

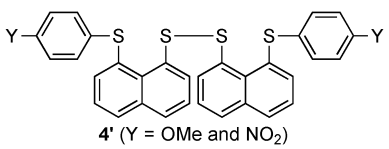

Chart 3 **4′** Having methoxy or nitro groups at phenyl *p*,*p′*-positions in **4**.

and **B** is very similar for **17** and **20** if calculated at the MP2 level. Scheme 5 summarizes the results.

If the reduction of **13–16** is started from the observed structures of **BA**, the **A** conformers are expected to form as the produced anions, **17–20**. However, the produced anions must be **B** for **18** and **19**, since they are more stable than **A**. This means that the **B** character will grow also in the transition states of **18** and **19**, which will stabilize the transition states of the reduction. Namely, the E–E bonds in **14** and **15** must be reduced more easily than the case of **13** and **16**. QC calculations explain well the observed results, since **14** and **15** corresponds to **2** and **3**, respectively, of which E–E bonds reduced easily.

Conclusion

Extended hypervalent bonds (*m*c–*n*e: $m \geq 4$) play an important role in physical, chemical and biological properties in the compounds containing the bonds. As the first step to elucidate the properties of $E_2E'_2$ 4c–6e, the structure, stability and reactivity of E′···E–E···E′ 4c–6e are examined for 1-(8-PhE′$C_{10}H_6$)EE($C_{10}H_6$E′Ph-8′)-1′ [**1** (E = Se, E′ = S), **2** (E = S, E′ = Se), **3** (E = E′ = Se) and **4** (E = E′ = S)], together with 1-$C_{10}H_7$EE$C_{10}H_7$-1′ [**5** (E = Se) and **6** (E = S)]. Linear alignments of four Se_2S_2 atoms in **1** and **2** are confirmed by the X-ray crystallographic analysis. The S–S bond in **2** is cleaved in the reduction with $NaBH_4$ in aqueous THF, whereas the Se–Se bond in **1** is not, contrary to the expectation. On the other hand, the Se–Se bond in **3** reacts with $NaBH_4$ under the same conditions, whereas the S–S bond in **4** is not. The reactivity of the E–E bond in **1–4** is not controlled by the central E atoms but by the outside E′ atoms.

QC calculations are performed on 1-(8-MeE′$C_{10}H_6$)EE-($C_{10}H_6$E′Me-8′)-1′ (**13–16**: models of **1–4**, respectively), **5** and **6**, together with the related species. **13** (**BA**), **15** (**BA**) and **16** (**BA**) containing $E_2E'_2$ 4c–6e are shown to be the global minima, which explain the observed structures. However, **14** (**AB**) containing double n(S)···σ*(Se–C) 3c–4e interactions is optimized to be the global minimum, although the observed structure in **2** correspond to **14** (**BA**). The important role of σ*(Se–C) to stabilize n(S)···σ*(Se–C) 3c–4e is well demonstrated by the QC calculations, containing the NBO analysis.

The reactivity of **13** and **14** can be directly examined since they are isomers with each other. **13** (**BA**) is the global minimum and **14** (**BA**) is most unstable in **13** and **14**: **13** (**BA**) is more stable than **14** (**BA**) by 62 kJ mol^{-1} at the MP2 level (Table 3). Therefore, the higher reactivity of **2** toward the reduction, relative to the negligible reactivity of **1**, is well explained by the lesser stability of **14** (**BA**) *vs.* higher stability of **13** (**BA**). The reactivity toward the reduction in **1–4** is also explained based on the stability of the produced anions (1-(8-MeE′$C_{10}H_6$)E^-).

Experimental

General considerations

Manipulations were performed under the nitrogen or argon atmosphere with standard vacuum-line techniques. Glassware was dried at 130 °C overnight. Solvents and reagents were purified by standard procedures as necessary. The melting points were determined on a Yanako MP-S3 melting point apparatus and are uncorrected. NMR spectra were recorded at 25 °C on a JEOL AL-300 spectrometer (^{1}H, 300 MHz; ^{13}C, 75.5 MHz; ^{77}Se, 57.3 MHz). The ^{1}H, ^{13}C and ^{77}Se chemical shifts are given in ppm relative to those of TMS for ^{1}H and ^{13}C NMR spectra and relative to reference compound MeSeMe for ^{77}Se NMR spectra. Column chromatography was performed with 300–400 mesh silica gel and basic alumina. Flash column chromatography was performed with 300–400 mesh silica gel and basic alumina and analytical thin layer chromatography was performed on precoated silica gel plates (60F-254) with the systems (v/v) indicated.

Naphtho[1,8-*c*,*d*]-1,2-selenathiole. This compound was prepared according to the literature.[33] 45% yield, Mp 122.5–123.5 °C, ^{1}H NMR (300 MHz, $CDCl_3$, δ, ppm, TMS): 7.18 (dd, ^3J(H,H) = 7.5 Hz, ^4J(H,H) = 1.1 Hz, 1H), 7.24 (*t*, ^3J(H,H) = 7.7 Hz, 1H), 7.24–7.32 (m, 2H), 7.35 (dd, ^3J(H,H) = 7.7 Hz, ^4J(H,H) = 1.1 Hz, 1H), 7.45 (dd, ^3J(H,H) = 6.8 Hz, ^4J(H,H) = 2.2 Hz, 1H); ^{77}Se NMR (57.3 MHz, $CDCl_3$, δ, ppm, MeSeMe): 561.6.

An almost equimolar mixture of **1** and **2** is obtained in the reaction of the naphtho[1,8-*c*,*d*]-1,2-selenathiolate dianion with excess benzenediazonium chloride in aqueous THF, at 5 °C. **1**, together with **7**, was isolated after the reduction of a mixture of **1** and **2** with $NaBH_4$ in ethanol.

Bis[8-(phenylthio)naphthyl] 1,1′-diselenide (1). 29% yield, mp 178.6–179.6 °C, ^{1}H NMR (300 MHz, $CDCl_3$, δ, ppm, TMS): 7.00–7.06 (m, 4H), 7.07–7.24 (m, 6H), 7.14 (t, ^3J(H,H) = 7.9 Hz, 2H), 7.48 (t, ^3J(H,H) = 7.7 Hz, 2H), 7.69 (dd, ^3J(H,H) = 8.1 and ^4J(H,H) = 0.9 Hz, 2H), 7.91 (dd, ^3J(H,H) = 8.1 and ^4J(H,H) = 1.3 Hz, 2H), 7.93 (dd, ^3J(H,H) = 7.5 and ^4J(H,H) = 1.1 Hz, 2H), 7.94 (dd, ^3J(H,H) = 8.1 and ^4J(H,H) = 1.1 Hz, 2H); ^{77}Se NMR (57.3 MHz, $CDCl_3$, δ, ppm, MeSeMe): 510.5. Anal. Calc. for **1** ($C_{32}H_{22}S_2Se_2$): C, 61.15; H, 3.53%. Found: C, 61.19; H, 3.60%.

1-(Methylthio)-8-(phenylselanyl)naphthalene (7). 64% yield, mp 85.5–86.5 °C, ^{1}H NMR (300 MHz, $CDCl_3$, δ, ppm, TMS): 2.56 (s, 3H), 7.12 (t, ^3J(H,H) = 7.7 Hz, 1H), 7.24 (dd, ^3J(H,H) = 7.6 and ^4J(H,H) = 1.4 Hz, 1H), 7.31–7.41 (m, 4H), 7.59–7.65 (m, 3H), 7.74 (dd, ^3J(H,H) = 8.6 and ^4J(H,H) = 1.5 Hz, 1H), 7.77 (dd, ^3J(H,H) = 7.3 and ^4J(H,H) = 1.4 Hz, 1H); ^{13}C NMR (75.0 MHz, $CDCl_3$, δ, ppm, TMS): 32.64, 125.55, 125.99, 127.37, 128.35, 129.54, 129.62, 130.74, 133.46, 133.61, 133.90, 133.97, 135.40, 135.96, 136.19; ^{77}Se NMR (57.3 MHz, $CDCl_3$, δ, ppm, MeSeMe): 457.2. Anal. Calc. for **7** ($C_{17}H_{14}SSe$): C, 62.00; H, 4.28%. Found: C, 61.74; H, 4.13%.

Bis[8-(phenylselanyl)naphthyl] 1,1′-disulfide (2). This compound was prepared by the reduction of 1-(8-PhSe$C_{10}H_6$)S_4($C_{10}H_6$SePh-8′)-1′ (**23**) with $NaBH_4$ in ethanol, **23** being prepared in the reaction of 1-Br-8-(PhSe)$C_{10}H_6$[10b] with magnesium in diethyl ether, followed by addition of sulfur. Recrystallization from $CHCl_3$ gave pure **2** in 22% yield. **2**: Mp 178.6–179.6 °C, ^{1}H NMR (300 MHz, $CDCl_3$, δ, ppm, TMS): 7.19 (t, ^3J(H,H) = 7.8 Hz, 2H), 7.27 (t, ^3J(H,H) = 7.7 Hz, 2H), 7.28–7.33 (m, 6H), 7.38 (dd, ^3J(H,H) = 7.5 and ^4J(H,H) = 1.3 Hz, 2H), 7.44

(dd, ^3J(H,H) = 7.4 and ^4J(H,H) = 1.3 Hz, 2H), 7.51–7.57 (m, 4H), 7.68 (dd, ^3J(H,H) = 8.1 and ^4J(H,H) = 1.1 Hz, 2H), 7.73 (dd, ^3J(H,H) = 8.1 and ^4J(H,H) = 1.3 Hz, 2H); ^{77}Se NMR (57.3 MHz, $CDCl_3$, δ, ppm, MeSeMe): 455.1. Anal. Calc. for **2** ($C_{32}H_{22}S_2Se_2$): C, 61.15; H, 3.53%. Found: C, 61.22; H, 3.62%.

X-Ray crystal structure determinations. Single crystals of **1** and **2** were obtained by slow evaporation of hexane at room temperature. X-Ray diffraction data for **1** and **2** were collected on a Rigaku/MSC Mercury CCD diffractometer equipped with a graphite-monochromated Mo-Kα radiation source (λ = 0.71070 Å). For **1**, the structure analysis is based on 4329 observed reflections with $I > 2.00\sigma(I)$ and 413 variable parameters; orange needles, 103 K, triclinic, space group $P\bar{1}$ (no. 2), a = 9.579(3), b = 11.979(4), c = 12.141(4) Å, α = 91.773(4), β = 102.912(4), γ = 110.758(2)°, V = 1260.5(7) Å^3, Z = 2, R = 0.020, R_w = 0.053, GOF = 1.000. For **2** the structure analysis is based on 4812 observed reflections with $I > 2.00\sigma(I)$ and 413 variable parameters; colorless needles, 103 K, triclinic, space group $C2/c$ (no. 15), a = 25.3639(5), b = 11.9664(4), c = 19.4789(6) Å, β = 118.9946(12)°, V = 5171.1(3) Å^3, Z = 8, R = 0.026, R_w = 0.057, GOF = 1.054. The structures were solved by direct method (SIR97),[34] and refined by full-matrix least-square method on F^2 for all reflections (SHELXL-97).[35]

CCDC reference numbers 626066 for **1** and 626067 for **2**.

For crystallographic data in CIF or other electronic format see DOI: 10.1039/b805678a

QC Calculations

Calculations are performed with the Gaussian 03 program.[22] The density functional theory (DFT) level of the Becke three parameter hybrid functionals with the Lee–Yang–Parr correlation functional (B3LYP)[23,24] are applied with the 6-311+G(d) basis sets being employed for Se and S and the 6-311G(d) basis sets for C and H. Frequency analysis is performed for each conformer at the B3LYP level. The Møller–Plesset second-order energy correlation (MP2) method[25] is also applied with the 6-311+G(d) basis sets for Se and S and the 4-31G(d) basis sets for C and H.

Acknowledgements

This work was partially supported by a Grant-in-Aid for Scientific Research (Nos. 16550038, 19550041 and 20550042) from the Ministry of Education, Culture, Sports, Science and Technology, Japan.

References

1 W. Nakanishi, *Hypervalent Chalcogen Compounds*, in *Handbook of Chalcogen Chemistry: New Perspectives in Sulfur, Selenium and Tellurium*, ed. F. A. Devillanova, Royal Society of Chemistry, Cambridge, 2007, ch. 10.3, pp. 644–668.

2 S. Alvarez, F. Mota and J. Novoa, *J. Am. Chem. Soc.*, 1987, **109**, 6586–6591; W. B. Farnham, D. A. Dixon and J. C. Calabrese, *J. Am. Chem. Soc.*, 1988, **110**, 8453–8461, see also J. C. Martin and M. M. Chau, *J. Am. Chem. Soc.*, 1974, **96**, 3319–3321.

3 (*a*) W. Nakanishi, S. Hayashi and S. Toyota, *Chem. Commun.*, 1996, 371–372; (*b*) W. Nakanishi, S. Hayashi and S. Toyota, *J. Org. Chem.*, 1998, **63**, 8790–8800; (*c*) S. Hayashi and W. Nakanishi, *J. Org. Chem.*, 1999, **64**, 6688–6696; (*d*) W. Nakanishi, S. Hayashi and T. Arai, *Chem. Commun.*, 2002, 2416–2417.

4 W. Nakanishi, S. Hayashi and N. Itoh, *Chem. Commun.*, 2003, 124–125; W. Nakanishi, S. Hayashi and N. Itoh, *J. Org. Chem.*, 2004, **69**, 1676–1684; W. Nakanishi, S. Hayashi, T. Furuta, N. Itoh, Y. Nishina, M. Yamashita and Y. Yamamoto, *Phosphorus, Sulfur Silicon Relat. Elem.*, 2005, **180**, 1351–1355; W. Nakanishi, S. Hayashi, S. Yamaguchi and K. Tamao, *Chem. Commun.*, 2004, 140–141.

5 (*a*) G. Mugesh, A. Panda, H. B. Singh, N. S. Punekar and R. J. Butcher, *Chem. Commun.*, 1998, 2227–2228; (*b*) G. Mugesh, A. Panda, H. B. Singh, N. S. Punekar and R. J. Butcher, *J. Am. Chem. Soc.*, 2001, **123**, 839–850; (*c*) J. E. Drake, M. B. Hursthouse, M. Kulcsar, M. E. Light and A. Silvestru, *Phosphorus, Sulfur Silicon Relat. Elem.*, 2001, **169**, 293–296; (*d*) J. E. Drake, M. B. Hursthouse, M. Kulcsar, M. E. Light and A. Silvestru, *J. Organomet. Chem.*, 2001, **623**, 153–160; (*e*) G. Mugesh, A. Panda, S. Kumar, S. Apte, H. B. Singh and R. J. Butcher, *Organometallics*, 2002, **21**, 884–892; (*f*) J. R. Anacona, J. Gomez and D. Lorono, *Acta Crystallogr., Sect. C*, 2003, **59**, o277–o280; (*g*) G. Mugesh, H. B. Singh and R. J. Butcher, *Eur. J. Inorg. Chem.*, 1999, 1229–1236; (*h*) G. Mugesh, H. B. Singh and R. J. Butcher, *J. Organomet. Chem.*, 1999, **577**, 243–248; (*i*) D. Shimizu, N. Takeda and N. Tokitoh, *Chem. Commun.*, 2006, 177–178.

6 *Molecular Interactions. From van der Waals to Strongly Bound Complexes*, ed. S. Scheiner, Wiley, New York, 1997; K. D. Asmus, *Acc. Chem. Res.*, 1979, **12**, 436–442; W. K. Musker, *Acc. Chem. Res.*, 1980, **13**, 200–206.

7 F. T. Burling and B. M. Goldstein, *J. Am. Chem. Soc.*, 1992, **114**, 2313–2320; Y. Nagao, T. Hirata, S. Goto, S. Sano, A. Kakehi, K. Iizuka and M. Shiro, *J. Am. Chem. Soc.*, 1998, **120**, 3104–3110; S. Wu and A. Greer, *J. Org. Chem.*, 2000, **65**, 4883–4887; Y. Nagao, H. Iimori, S. Goto, T. Hirata, S. Sano, H. Chuman and M. Shiro, *Tetrahedron Lett.*, 2002, **43**, 1709–1712; E. Meyer, A. C. Joussef, H. Gallardo, A. J. Bortoluzzi and R. L. Longo, *Tetrahedron*, 2003, **59**, 10187–10193; Y. Nagao, T. Honjo, H. Iimori, S. Goto, S. Sano, M. Shiro, K. Yamaguchi and Y. Sei, *Tetrahedron Lett.*, 2004, **45**, 8757–8761; J. C. Taylor and G. D. Markham, *J. Biol. Chem.*, 1999, **274**, 32909–32914; W. Brandt, A. Golbraikh, M. Täger and U. Lendeckel, *Eur. J. Biochem.*, 1999, **261**, 89–97.

8 V. Lippolis and F. Isaia, *Charge-Transfer (C.-T.) Adducts and Related Compounds*, in *Handbook of Chalcogen Chemistry: New Perspectives in Sulfur, Selenium and Tellurium*, ed. F. A. Devillanova, Royal Society of Chemistry, Cambridge, 2006, ch. 8.2, pp. 477–499C. Rêthorê, M. Fourmiguê and N. Avarvari, *Chem. Commun.*, 2004, 1384–1385; C. Rêthorê, M. Fourmiguê and N. Avarvari, *Tetrahedron*, 2005, **61**, 10935–10942; C. Rêthorê, N. Avarvari, E. Canadell, P. Auban-Senzier and M. Fourmiguê, *J. Am. Chem. Soc.*, 2005, **127**, 5748–5749.

9 C. Rêthorê, A. Madalan, M. Fourmiguê, E. Canadell, E. B. Lopes, M. Almeida, R. Clêrac and N. Avarvari, *New J. Chem.*, 2007, **31**, 1468–1483.

10 (*a*) W. Nakanishi, S. Hayashi and T. Uehara, *J. Phys. Chem. A*, 1999, **103**, 9906–9912; (*b*) W. Nakanishi, S. Hayashi and T. Uehara, *Eur. J. Org. Chem.*, 2001, 3933–3943; (*c*) W. Nakanishi and S. Hayashi, *J. Org. Chem.*, 2002, **67**, 38–48; (*d*) S. Hayashi, H. Wada, T. Ueno and W. Nakanishi, *J. Org. Chem.*, 2006, **71**, 5574–5585.

11 G. C. Pimentel, *J. Chem. Phys.*, 1951, **19**, 446–448; J. I. Musher, *Angew. Chem., Int. Ed. Engl.*, 1969, **8**, 54–68; R. A. Hayes and J. C. Martin, in *Sulfurane Chemistry in Organic Sulfur Chemistry: Theoretical and Experimental Advances*, eds. F. Bernardi, I. G. Csizmadia and A. Mangini, Elsevier, Amsterdam, 1985*Chemistry of Hypervalent Compounds*, ed. K.-Y. Akiba, Wiley-VCH, New York, 1999.

12 W. Nakanishi, S. Hayashi, A. Sakaue, G. Ono and Y. Kawada, *J. Am. Chem. Soc.*, 1998, **120**, 3635–3640.

13 S. Kumar, K. Kandasamy, H. B. Singh and R. J. Butcher, *New J. Chem.*, 2004, **28**, 640–645.

14 R.-F. Hu, Y.-H. Wen, J. Zhang, Z.-J. Li and Y.-G. Yao, *Acta Crystallogr., Sect. E*, 2004, **60**, o2029–o2031; S. Wang, H. Mao-Lin and F. Chen, *Acta Crystallogr., Sect. E*, 2004, **60**, m413–m415; X.-J. Wang, Z.-F. Chen, B.-S. Kang, H. Liang, H.-Q. Liu, K.-B. Yu, C.-Y. Su and Z.-N. Chen, *Polyhedron*, 1999, **18**, 647–655.

15 J. C. Barnes, J. D. Paton, W. Schroth and L. Moegel, *Acta Crystallogr., Sect. B*, 1982, **38**, 1330–1332; D. J. Dahm, F. L. May, J. J. D'Amico, C. C. Tung and R. W. Fuhrhop, *Cryst. Struct. Commun.*, 1977, **6**, 393.

16 T. C. W. Mak, W.-H. Yip, W.-H. Chan, G. Smith and C. H. L. Kennard, *Aust. J. Chem.*, 1989, **42**, 1403–1406.
17 The structures of **3** (E = E′ = Se) and **4** (E = E′ = S) were determined by the X-ray crystallographic analysis:[3a,b,d] Four E atoms in **3** and **4** align linearly among a lot of possibilities with the free rotation around the C–Se and C–S bonds, respectively.
18 P. G. Jones, C. Kienitz and C. Thone, *Z. Kristallogr.*, 1994, **209**, 83–84.
19 Details will be reported elsewhere.
20 The reactivity of **2** is examined carefully, using the compound independently prepared.
21 A. Bondi, *J. Phys. Chem.*, 1964, **68**, 441–451.
22 M. J. Frisch, G. W. Trucks, H. B. Schlegel, G. E. Scuseria, M. A. Robb, J. R. Cheeseman, J. A. Montgomery, Jr, T. Vreven, K. N. Kudin, J. C. Burant, J. M. Millam, S. S. Iyengar, J. Tomasi, V. Barone, B. Mennucci, M. Cossi, G. Scalmani, N. Rega, G. A. Petersson, H. Nakatsuji, M. Hada, M. Ehara, K. Toyota, R. Fukuda, J. Hasegawa, M. Ishida, T. Nakajima, Y. Honda, O. Kitao, H. Nakai, M. Klene, X. Li, J. E. Knox, H. P. Hratchian, J. B. Cross, V. Bakken, C. Adamo, J. Jaramillo, R. Gomperts, R. E. Stratmann, O. Yazyev, A. J. Austin, R. Cammi, C. Pomelli, J. W. Ochterski, P. Y. Ayala, K. Morokuma, G. A. Voth, P. Salvador, J. J. Dannenberg, V. G. Zakrzewski, S. Dapprich, A. D. Daniels, M. C. Strain, O. Farkas, D. K. Malick, A. D. Rabuck, K. Raghavachari, J. B. Foresman, J. V. Ortiz, Q. Cui, A. G. Baboul, S. Clifford, J. Cioslowski, B. B. Stefanov, G. Liu, A. Liashenko, P. Piskorz, I. Komaromi, R. L. Martin, D. J. Fox, T. Keith, M. A. Al-Laham, C. Y. Peng, A. Nanayakkara, M. Challacombe, P. M. W. Gill, B. Johnson, W. Chen, M. W. Wong, C. Gonzalez and J. A. Pople, *GAUSSIAN 03 (Revision B.05)*, Gaussian, Inc., Pittsburgh, PA, 2003.
23 C. Lee, W. Yang and R. G. Parr, *Phys. Rev. B*, 1988, **37**, 785–789; B. Miehlich, A. Savin, H. Stoll and H. Preuss, *Chem. Phys. Lett.*, 1989, **157**, 200–2006.
24 A. D. Becke, *Phys. Rev. A*, 1988, **38**, 3098–3100; A. D. Becke, *J. Chem. Phys.*, 1993, **98**, 5648–5652.
25 C. Møller and M. S. Plesset, *Phys. Rev.*, 1934, **46**, 618–622; J. Gauss, *J. Chem. Phys.*, 1993, **99**, 3629–3643; J. Gauss, *Ber. Bunsenges, Phys. Chem.*, 1995, **99**, 1001–1008.
26 A. E. Reed, R. B. Weinstock and F. Weinhold, *J. Chem. Phys.*, 1985, **83**, 735–746; J. E. Carpenter and F. Weinhold, *J. Mol. Struct. (THEOCHEM)*, 1988, **169**, 41–62.
27 NBO Ver. 3.1, E. D. Glendening, A. E. Reed, J. E. Carpenter and F. Weinhold.
28 The accuracy of the calculated bond lengths for the classical bonds and the nonbonded distances with the method employed in this work would be around 0.01 and 0.1 Å, respectively. However, the accuracy for the differences between conformers must be higher. Therefore, the predicted r(Se···S) differences of 0.046 (B3LYP) and 0.066 Å (MP2) would explain the observed values of 0.075 Å, although the Ph groups in **1–4** are replaced by the Me groups in **13–16** (Table 2). The discussion on the accuracy of the energies seems more delicate. Therefore, we usually discuss the differences between those of the conformational isomers.[36] In our cases, the differences make some sense if they are larger than several kJ mol^{-1}, although they depend on the calculation method.[37] It is better to compare a series of differences (not between only two), as shown in Tables 3–5. The crystal packing effect and/or solvent effect must also be considered when the values are compared with the experimental results.
29 The results suggest that **2** (**BA**) and **2** (**AB**) may be in equilibrium in solutions.
30 For the structures of **5** and **6**, see CCDC-611300 (**5**) and CCDC-611301 (**6**)[19]
31 The process also contains the change from double p(E′)–π(Nap) to double p(E)–π(Nap) interactions.
32 The charges at E and E′ are also very important to understand the formation of n_p(E′)···σ*(E–E)···n_p(E′) 4c–6e in **BA** and the n_p(E)···σ*(E′–C) 3c–4e in **AB**.[3] However, it is difficult to discuss directly based on the values, since they are mainly determined by the conformers, **A** or **B**. Details will be discussed elsewhere.
33 J. Meinwald and D. Dauplaise, *J. Am. Chem. Soc.*, 1977, **99**, 7743.
34 A. Altomare, M. C. Burla, M. Camalli, G. L. Cascarano, C. Giacovazzo, A. Guagliardi, A. G. G. Moliterni, G. Polidori and R. Spagna, *J. Appl. Crystallogr.*, 1999, **32**, 115–119.
35 G. M. Sheldrick, SHELXL-97, Program for the Refinement of Crystal Structures, University of Göttingen, Göttingen, 1997.
36 This idea is well supported by the high accuracy in the calculations for the isodesmic reaction. See, J. B. Foresman and A. E. Frisch, *Exploring Chemistry with Electronic Structure Methods*, Gaussian Inc, Pittsburg, PA, 2nd edn, 1996, ch. 8.
37 **1** (**BA**) and **2** (**BA**) are optimized employing the 6-311G(d) basis sets for S and Se and the 4-31G basis sets for C and H. The former is predicted to be more stable than the latter by 70.9 kJ mol^{-1} with r(S···Se) of **1** (**BA**) being shorter than that of **2** (**BA**) by 0.052 Å.